

# Starvation insult induces the translocation of high mobility group box 1 to cytosolic compartments in glioma

XIAOHANG CUI<sup>1\*</sup>, ANHUI YAO<sup>2\*</sup> and LIYUN JIA<sup>1</sup>

<sup>1</sup>Department of Medical Genetics and Cell Biology, School of Basic Medical Sciences, Zhengzhou University, Zhengzhou, Henan 450001; <sup>2</sup>Department of Neurosurgery, 988th Hospital of Joint Logistic Support Force of PLA, Zhengzhou, Henan 450053, P.R. China

Received May 3, 2023; Accepted October 4, 2023

DOI: 10.3892/or.2023.8653

**Abstract.** High mobility group box 1 (HMGB1) is a highly conserved and ubiquitous nuclear protein in eukaryotic cells. In response to stress, it transfers from the nucleus to the cytoplasm and finally, to the extracellular matrix, participating in inflammation and carcinogenesis. Increased HMGB1 protein levels are frequently associated with the reduced survival of patients with glioma. HMGB1 plays contextual roles depending on its subcellular localization. However, the mechanisms underlying its subcellular localization and secretion remain unclear. In the present study, the subcellular localization and secretion of HMGB1 in starved glioma cells were investigated using immunofluorescence microscopy, enzyme-linked immunosorbent assay, subcellular fractionation, western blotting and immunoelectron microscopy. The results demonstrated that starvation induced HMGB1 translocation from the nucleus to the cytoplasm and finally, to the extracellular milieu in glioma cells. HMGB1 was localized in the mitochondria, endoplasmic reticulum (ER), peroxisomes, autophagosomes, lysosomes, endosomes and the cytoskeleton. Immunoelectron microscopy confirmed that HMGB1 was present within or around cytosolic compartments. Subcellular fractionation further demonstrated that HMGB1 transferred to membrane-bound compartments. In addition, HMGB1 was localized to specific contact areas between the ER and mitochondria, known as mitochondria-associated membranes. On the whole, the results of the present study suggest that starvation induces HMGB1 secretion, which can be inhibited through the suppression of autophagy. Starvation insult induces HMGB1 translocation

to the cytosolic compartments of glioma cells, and autophagy may be involved in the extracellular secretion of HMGB1 in starved glioma cells.

## Introduction

Gliomas are the most prevalent primary brain tumors, representing 81% of malignant brain tumors. According to the classification of the World Health Organization (WHO), gliomas can be divided into four grades: Grades I and II corresponding to low-grade gliomas, and grades III and IV corresponding to high-grade gliomas (1). Generally, relatively high grades are associated with a poor prognosis. The median overall survival (OS) of patients with grade III glioma is ~3 years, whereas that of patients with grade IV glioma is only 15 months (2,3). Elucidating the molecular mechanisms underlying the tumorigenesis of gliomas is critical in order to improve the therapeutic efficacy of glioma treatment and prolong the OS of patients.

High mobility group box 1 (HMGB1) is a non-histone DNA-binding protein mainly located in the nucleus of eukaryotic cells under homeostatic conditions. In response to stress, it translocates from the nucleus to the cytoplasm and is released from the cell (4). HMGB1 participates in various cellular functions, mainly depending on its subcellular localization (4). In the cytoplasm, HMGB1 induces autophagy by binding to Beclin-1 and regulates mitochondrial quality (5). In the extracellular matrix, HMGB1 functions as a damage-associated molecule that participates in multiple cellular activities, including cell-cell interactions, pro-inflammatory cytokine production, cell proliferation, differentiation, invasion and autophagy (4,6). The dysregulation of HMGB1 has been shown to be associated with a number of diseases, particularly cancer. In solid tumors, HMGB1 usually translocates from the nucleus to the cytoplasm (6). High levels of HMGB1 have been observed in various types of malignancies, including lung cancer, breast cancer, head and neck squamous cell carcinoma, colon cancer, nasopharyngeal carcinoma and glioma (7-10). Extracellular HMGB1 can function as a paracrine or autocrine factor to drive tumor growth, proliferation, migration and angiogenesis (11). HMGB1 expression is frequently upregulated in gliomas. Its overexpression is associated with glioma progression and a poor prognosis (12,13). The transcription and

*Correspondence to:* Dr Liyun Jia, Department of Medical Genetics and Cell Biology, School of Basic Medical Sciences, Zhengzhou University, Kexue Avenue 100, Zhengzhou, Henan 450001, P.R. China  
E-mail: jialiyun0410@zzu.edu.cn

\*Contributed equally

**Key words:** glioma, high mobility group box 1, starvation, translocation, secretion, membrane-bound compartments

translocation of HMGB1 from the nucleus to the cytoplasm mediate autophagy and glioma growth (12). It has been demonstrated that extracellular HMGB1 released by patient-derived glioma cells following temozolomide (TMZ) treatment increases the formation of glioma stem cells, which further induce resistance to TMZ (14). Controversially, Li *et al* (15) revealed that the unconventional autophagy-based secretion of HMGB1 in glioblastoma promoted chemosensitivity to TMZ through macrophage polarization. Thus, the translocation and release of HMGB1 from glioma cells are crucial steps in glioma progression. However, the exact mechanisms by which HMGB1 is translocated and the precise subcellular pathway of HMGB1 in gliomas during its release are poorly understood.

The microenvironment in solid tumors is poor in nutrients and glucose-deprived, owing to the high rate of tumor cell consumption (16). Cancer cell proliferation is dependent on extracellular nutrient acquisition; however, glucose, amino acids and lipids are usually in short supply, due to inadequate tumor perfusion (17). Nutrient deficiency is closely related to metabolic changes in tumor cells and promotes tumorigenesis. Therefore, in the present study, the subcellular localization and secretion of HMGB1 in starved glioma cells were investigated, in order to clarify the translocation and release pathways of HMGB1 in glioma cells under nutrient-poor conditions. It was revealed that HMGB1 translocated from the nucleus to the cytoplasm and was then secreted into the exterior of starved glioma cells. HMGB1 in the cytoplasm was distributed within or around the mitochondria, endoplasmic reticulum (ER), peroxisomes, autophagosomes, early endosomes, late endosomes, lysosomes, cytoskeleton and mitochondria-associated ER membranes (MAMs). The Manders' overlap coefficient of HMGB1 in these compartments was markedly altered upon its release. In addition, autophagy mediated the release of HMGB1 in starved glioma cells. The findings of the present study provided a novel perspective to further clarify the mechanisms by which HMGB1 affects gliomas under starvation.

## Materials and methods

**Cases.** A total of six glioma and three normal brain tissue sections (human samples isolated during decompression operations) were obtained from the Department of Histology at the 988th Hospital of the Joint Logistic Support Force (Zhengzhou, China). Additionally, glioblastoma tissue (male, 66 years old) obtained from the Department of Neurosurgery of the same hospital was used for transmission electron microscopy. The age range and median age of the patients were 36 to 66 years and 52.7 years, respectively. The WHO grade, sex and age of all seven glioma cases are listed in Table SI. The isolated tissues were first fixed in 4% paraformaldehyde (PFA) at 4°C for 24 h before the subsequent treatments. The entire storage process, from isolation to storage, was completed within 30 min. Glioma samples were validated by experienced clinical pathologists in the hospital in accordance with the WHO classification (2016) (18). Written informed consent was obtained from all patients with glioma and the families of the three patients with traumatic brain injury who underwent decompression surgery. The present study was conducted in accordance with the Declaration of Helsinki, and the protocol was approved

by the Ethics Committee of the 988th Hospital of the Joint Logistic Support Force (Zhengzhou, China).

**Cells and reagents.** HA1800 astrocytes were purchased from Shanghai Ji Ning Industrial Co., Ltd., and three human glioma cell lines [U251, U87-MG (ATCC version, glioblastoma of unknown origin and U118-MG)] were purchased from The Cell Bank of Type Culture Collection of the Chinese Academy of Sciences. Mycoplasma testing was performed on the cell lines (data not shown), and the cells were authenticated using STR profiling. The cells were sub-cultured in Dulbecco's modified Eagle's medium (Biological Industries; cat. no. C3110-0500) supplemented with 10% fetal bovine serum (BSA; Biological Industries; cat. no. 04-001-1ACS) and 1% penicillin-streptomycin (Beijing Solarbio Science & Technology Co., Ltd.; cat. no. P1400) and maintained in 5% CO<sub>2</sub> at 37°C in a humidified incubator. The glioma cells were treated with Hank's balanced salt solution (HBSS; Beijing Solarbio Science & Technology Co., Ltd.; cat. no. H1025) at the indicated time intervals (0, 0.5, 1, 2, 3 and 4 h) for starvation stress induction or H<sub>2</sub>O<sub>2</sub> (300 µM; Laiyang City Shuangshuang Chemical Co., Ltd.) for 4 h for oxidative stress. Wortmannin (WOR; Shanghai Selleck Chemicals Co., Ltd.; cat. no. S2758; 0.5 µM) and chloroquine (CQ; Shanghai Selleck Chemicals Co., Ltd.; cat. no. S6999; 20 µM) were used to inhibit early and late autophagy, respectively. U251 glioma cells were pretreated with WOR or CQ for 2 h and then stimulated with or without HBSS for 3 h in the presence of WOR or CQ at 37°C in a humidified incubator.

**Cell transfection.** The cells were cultured in six-well culture plates until they reached 80% confluency, after which they were transfected with 2 µg pEGFP-C1 or the HMGB1 recombinant overexpression plasmid pEGFP-HMGB1-C1 (Shanghai Sangon Biotech Co., Ltd.) using Simple-Fect Transfection Reagent (Zhengzhou Kebang Biological Technology Co., Ltd.) for 16 h at 37°C in a humidified incubator in accordance with the manufacturer's protocol. The culture medium was then switched to a normal medium. After ~24 h, the experiments described in the following sections were conducted.

**Immunohistochemistry (IHC).** IHC was performed as previously described (19). Briefly, deparaffinized glioma slices (5-µm-thick) were permeabilized with 0.3% Triton X-100 (Beijing Biotopped Co., Ltd.; cat. no. T6200G) in PBS for 20 min at room temperature (RT). Subsequently, the cells were blocked with blocking solution [5% BSA (Beijing Solarbio Science & Technology Co., Ltd.; cat. no. A8020)] plus 0.3% Triton X-100 in phosphate-buffered saline (PBS) for 1 h at RT. Subsequently, the cells were incubated with anti-HMGB1 (Abcam; cat. no. ab18256; 1:500), anti-ATP synthase F1 subunit alpha (ATP5A; Abcam; cat. no. ab14748; 1:200), anti-Lysosomal-associated membrane protein 1 (LAMP1; CST Biological Reagents Co., Ltd.; cat. no. 9091#; 1:100), anti-Ras-related protein 5 (Rab-5; Abcam; cat. no. ab18211; 1:200), anti-glial fibrillary acidic protein [(GFAP; Abcam; cat. no. ab279290; 1:500) and anti-calnexin (CANX) antibodies sMilliporeSigma; cat. no. SAB2501291; 1:200] overnight at 4°C. All sections were rinsed with PBS and then incubated with the following fluorescein-conjugated secondary antibodies for 2 h at RT: Fluorescein-conjugated goat anti-rabbit

IgG (H+L) (Beijing ZSGB-BIO Co. Ltd.; cat. no. ZF-0311; 1:100), Alexa Fluor 488 donkey anti-rabbit IgG (H+L) (Abcam; cat. no. ab150073; 1:500), rhodamine-conjugated goat anti-mouse IgG (H+L) (Beijing ZSGB-BIO Co. Ltd; cat. no. ZF-0313; 1:100) and Alexa Fluor 633 donkey anti-goat IgG (H+L) (Invitrogen Trading Shanghai Co. Ltd; cat. no. A-21082; 1:500). Nuclei were stained with 4'-6-diamidino-2-phenylindole (DAPI; Beijing Solarbio Science & Technology Co., Ltd.; cat. no. C0060; 1:5,000) for 15 min at RT. Images were acquired using an Olympus confocal microscope (LSM; cat. no. FV1000; Olympus Corporation) and analyzed using Adobe Photoshop CS6 (Adobe Systems, Inc.; version 13.0.1x64) and ImageJ software (National Institutes of Health; version 1.4.3.67).

**Immunocytochemistry (ICC).** ICC was performed as previously described (19). Following appropriate treatment with HBSS, the cells were washed twice with ice-cold PBS, fixed with freshly prepared 4% PFA in PBS for 15 min at RT, and then permeabilized with 0.3% Triton X-100 (Beijing Biotopped Co., Ltd.; cat. no. T6200G) in PBS for 20 min at RT. Subsequently, the cells were blocked with blocking solution (as mentioned for IHC) for 1 h at RT and then incubated with the following primary antibodies overnight at 4°C: Anti-HMGB1 (Abcam; cat. no. ab18256; 1:1,000), anti-LAMP1 (China-based branch, CST Biological Reagents Co., Ltd.; cat. no. 9091; 1:500), anti-microtubule-associated proteins 1A/1B light chain 3B (LC3B; CST Biological Reagents Co., Ltd.; cat. no. 3868; 1:500), anti-catalase (Abcam; cat. no. ab16731; 1:200), anti-CANX (MilliporeSigma; cat. no. SAB2501291; 1:500), anti-Rab5 (Abcam; cat. no. ab18211; 1:500), anti-Rab7 (Abcam; cat. no. ab137029; 1:500), anti-GFAP (Abcam; cat. no. ab279290; 1:500) and anti-Sigma 1 receptor (Sigma1-R) antibodies (Abcam; cat. no. ab53852; 1:100). The cells were incubated with the secondary antibodies used in IHC for 2 h at RT and then counterstained with DAPI at RT for 15 min. In several experiments, cells were preloaded with MitoTracker Red CMXRos for 25 min at 37°C in a humidified incubator before fixation to label the mitochondria (Thermo Fisher Scientific, Inc.; cat. no. M7512). Images were obtained by Olympus confocal microscope and analyzed using Adobe Photoshop CS6 (Adobe Systems, Inc.; version 13.0.1x64) and ImageJ software (National Institutes of Health; version 1.4.3.67).

**Enzyme-linked immunosorbent assay (ELISA).** Cell supernatants were collected and assayed using an HMGB1 ELISA kit (Cusabio Technology, LLC; cat. no. CSB-E08223h) in accordance with the manufacturer's instructions. Briefly, 100 µl standards or samples were added to each well for 2 h at 37°C. Following the removal of the liquid, 100 µl biotin-conjugated HMGB1 antibody (Cusabio Technology, LLC; cat. no. CSB-E08223h) was added with for 1 h at 37°C and then washed three times with wash buffer. Horseradish peroxidase-conjugated goat anti-rabbit IgG (Cusabio Technology, LLC; cat. no. CSB-E08223h) was added for 1 h at 37°C. After being washed five times, 90 µl of 3,3',5,5'-tetramethylbenzidine substrate were added to each well and the plate was incubated for 30 min at 37°C. The reaction was terminated by adding 50 µl of stop solution, and the optical density was then read

at 450 nm using a microplate tester (Multiskan Mk3, Thermo Fisher Scientific, Inc.) within 5 min.

**Immunoelectron microscopy.** Glioma cells were harvested and immediately fixed in 4% glutaraldehyde in 0.1 M phosphate buffer (pH 7.4) and incubated for 2 h at 4°C. Following centrifugation at 100 x g for 5 min at 4°C, samples immersed in 4% glutaraldehyde in 0.1 M phosphate buffer (pH 7.4) were sent to the biomedical testing center of Tsinghua University, and the remaining steps were performed. The samples were coated with 4 nm gold and viewed in a JEM-1400 electron microscope (JEOL, Ltd.).

**Western blotting (WB).** Glioma cells were lysed in RIPA lysis buffer (Beijing Solarbio Science & Technology Co., Ltd.; cat. no. R0010). The protein amounts in the whole-cell lysates were determined using the BCA Protein Assay kit (Beijing Solarbio Science & Technology Co., Ltd.; cat. no. PC0020). In total, 20-50 µgs protein extracts were separated on a 12% SDS-PAGE and then transferred to polyvinylidene fluoride membranes (MilliporeSigma; cat. no. IPVH00010). Following blocking with 5% non-fat dry milk solution (in Tris-buffered saline wash buffer with 1% Tween-20) for 1 h at RT, the membranes were probed overnight at 4°C with the following primary antibodies: Anti-HMGB1 (Abcam; cat. no. ab18256; 1:1,000), anti-CANX (MilliporeSigma; cat. no. SAB2501291; 1:500), anti-ATP5A (Abcam; cat. no. ab14748; 1:1,000), anti-β-actin (OriGene Technologies, Inc.; cat. no. TA-09; 1:2,000), anti-LaminB1 (China-based branch, Cell Signaling Technology, Inc.; cat. no. 13435; 1:1,000), anti-LC3B (Cell Signaling Technology, Inc. 3868; 1:1,000), anti-GAPDH (Hangzhou Xianzhi Biological Technology Co., Ltd.; cat. no. AB-P-R 001; 1:1,000), and anti-p62 (China-based branch, Cell Signaling Technology, Inc.; cat. no. 23214, 1:1,000). Subsequently, the membranes were incubated with peroxidase-conjugated goat anti-mouse or anti-rabbit IgG secondary antibodies (Beijing ZSGB-BIO Co. Ltd; cat. no. ZB-2305 or ZB-2301, respectively; 1:5,000) for 2 h at RT. An enhanced chemiluminescent substrate (Dalian Meilun Biology Technology Co., Ltd.; cat. no. MA0186) was used to visualize the protein bands. Relative band intensities were quantified using ImageJ software (National Institutes of Health; version 1.4.3.67).

**Subcellular fractionation.** U87-MG glioma cells in 10 dishes, 10 cm each, were treated with HBSS (Beijing Solarbio Science & Technology Co., Ltd.; cat. no. H1025) for 1 h at 37°C and then harvested in lysis buffer [20 mM HEPES-KOH (pH 7.2, Sigma-Aldrich (Shanghai) Trading Co.Ltd., cat. no. V900477), 400 mM sucrose (Beijing Solarbio Science & Technology Co., Ltd.; cat. no. S8271), and 1 mM EDTA (Beijing Solarbio Science & Technology Co., Ltd.; cat. no. E8030)] supplemented with protease and phosphatase inhibitor (Dalian Meilunbio Co. Ltd., cat. no. MB12707-1) and 0.3 mM dithiothreitol (Beijing Solarbio Science & Technology Co., Ltd.; cat. no. D8220). The cell lysates were then homogenized by using a 22G needle. The homogenates were centrifuged at 800 x g for 10 min at RT to pellet the nuclei and cytoskeleton. The ER, crude mitochondria, and pure mitochondria in the cytoplasm were fractionated following previously described protocols, and analyzed using WB (20). Anti-CANX (MilliporeSigma; cat. no. SAB2501291;

1:500) antibody and ATP5A (Abcam; cat. no. ab14748; 1:200) were used as markers for the ER and pure mitochondria proteins, respectively. Autophagosomes were fractionated following the method described by Zhang *et al.* (21). The homogenates were sequentially centrifuged at 3,000 x g for 10 min, 25,000 x g for 20 min, and 100,000 x g for 30 min at RT (TLA100.3 rotor; Beckman Coulter, Inc.), and the pelleted membranes were collected at each speed, and analyzed using WB. Anti-LC3B antibody (CST Biological Reagents Co., Ltd.; cat. no. 3868; 1:500) was used as marker for the autophagosomes.

**Protease K protection assay.** The pelleted membranes that were previously centrifuged at 25,000 x g and 100,000 x g were resuspended in buffer containing 25 µg/ml protease K [Sigma-Aldrich (Shanghai) Trading Co. Ltd., cat. no. 3115828001], with or without 1% Triton X-100 (Beijing Biotopped Co., Ltd.; cat. no. T6200G) and then incubated on ice for 30 min. The reaction was terminated by adding 5X SDS loading buffer (Beijing Dingguo Changsheng Biotechnology Co., Ltd., cat. no. WB-0091), heated in boiling water for 10 min, and analyzed using WB.

**Lactate dehydrogenase (LDH) release assay.** LDH release was measured as a physiological index of cell membrane damage. U87-MG glioma cells were treated with HBSS to induce starvation stress at the indicated time intervals (0, 0.5, 1, 2, 3 and 4 h). U251 glioma cells were stimulated with or without HBSS (3 h), WOR (3 h, 0.5 µM), or CQ (3 h, 20 µM). The release of LDH from these cells was measured using an LDH cytotoxicity assay kit (Beyotime Institute of Biotechnology; cat. no. C0016) in accordance with the manufacturer's instructions. Briefly, the supernatant of the treated glioma cells was collected and added with LDH reagent. The mixture was incubated in the dark for 30 min at RT, and the OD490 value was measured using a microplate tester (Multiskan Mk3, Thermo Fisher Scientific, Inc.).

**Cell Counting Kit-8 (CCK-8) assay.** Cell viability was assessed using the CCK-8 assay (Dalian Meilun Biotech Co., Ltd.; cat. no. MA0218-5) following the manufacturer's protocol. Briefly, cells were seeded in 96-well plates and grown to 80% confluency. In total, a quantity of 10 µl CCK-8 reagent was added to the treated glioma cells and incubated for 2 h at 37°C in a humidified incubator with 5% CO<sub>2</sub>. The absorbance was obtained at 450 nm using a microplate tester (Multiskan Mk3, Thermo Fisher Scientific, Inc.).

**Statistical analysis.** All assays were performed independently and at least in triplicate. Statistical results are expressed as mean ± SD. An unpaired Student's t-test and one-way analysis of variance (ANOVA) followed by Tukey's post-hoc test were used for statistical analyses using GraphPad Prism software (Dotmaticx; Version 8.3.0.538). Manders' overlap coefficient was calculated using the JACoP ImageJ plugin (National Institutes of Health; version 1.4.3.67) as previously described (22). Line fluorescence tracing from the images was performed using OriginPro software (OriginLab; version 8.5). P<0.05 was considered to indicate a statistically significant difference.

## Results

**Translocation of HMGB1 in glioma cells.** To examine the translocation of HMGB1, its distribution was first analyzed in normal and glioma tissues. As presented in Fig. 1, HMGB1 was mainly distributed in the nucleus of the normal brain tissues (Fig. 1A), whereas in the glioma tissues, it was localized in the nucleus and cytoplasm (Fig. 1B and C). In certain cells, the distribution of HMGB1 solely inside the cytoplasm was observed (Fig. 1C). The difference in the localization of HMGB1 demonstrated in Fig. 1B and C was potentially due to glioma heterogeneity. The cytoplasmic HMGB1 localization index of HMGB1 has been shown to be moderately associated with tumor stage in a previously published study on cholangiocarcinoma (23). HMGB1 is mainly localized to the nucleus under homeostatic conditions (24). In the present study, when the cells were treated with HBSS (starvation), HMGB1 was released from the nucleus into the cytoplasm and extracellular medium (Fig. 2A-C). The cytoplasmic expression of HMGB1 reached its maximum 1 h after HBSS treatment (Fig. 2B), whereas its extracellular secretion reached its maximum at 2 h (Fig. 2C). LDH release assay revealed that the increase in HMGB1 secretion was not attributed to non-specific membrane permeability (Fig. 2D).

**Co-localization of HMGB1 and specific marker proteins of cellular compartments in glioma.** The association between HMGB1 and the cytosolic compartments was then investigated and the subcellular localization of HMGB1 was determined using ICC. The results revealed that HMGB1 co-localized with Mitotracker Red, CANX, catalase, LC3B, LAMP1, Rab5 and Rab7, indicating that HMGB1 was imported into the mitochondria, ER, peroxisomes, autophagosomes, lysosomes, early endosomes and late lysosomes of glioma cells. Oxidative stress with H<sub>2</sub>O<sub>2</sub> was also induced the HMGB1 translocation to the cytoplasm and colocalization with Mitotracker Red in glioma cells (Fig. S1A and B). Furthermore, merged images of HMGB1 with GFAP were obtained, indicating that HMGB1 was associated with the cytoskeleton in glioma cells (Figs. 3A and B, and 4A and B). Notably, the staining of GFAP in the glioma cells did not reveal the cytoskeleton-like structure, as was expected. A similar result has been confirmed in previous studies (25,26). This finding may be attributed to the moderate immune response of glioma cells to GFAP (27).

In order to explore the association of HMGB1 with these compartments during secretion, Manders' overlap coefficient between HMGB1 and the aforementioned marker proteins were analyzed, and compared at 1 and 3 h following starvation. Manders' overlap coefficient, which is commonly used to examine protein co-localization (28,29), ranged between 0 and 1 in the present study. The higher the Manders' overlap rate, the higher the fluorescence overlap rate. The results demonstrated that the Manders' overlap coefficient between HMGB1 and MitoTracker Red, LC3B, LAMP1 and Rab7 was significantly lower at 3 h than at 1 h following starvation, whereas that between HMGB1 and catalase or GFAP increased (Figs. 3C and 4C). The change in the Manders' overlap coefficient suggests that HMGB1 is dynamically associated with cytoplasmic compartments in starved glioma cells. In addition, the subcellular localization of HMGB1 was examined in



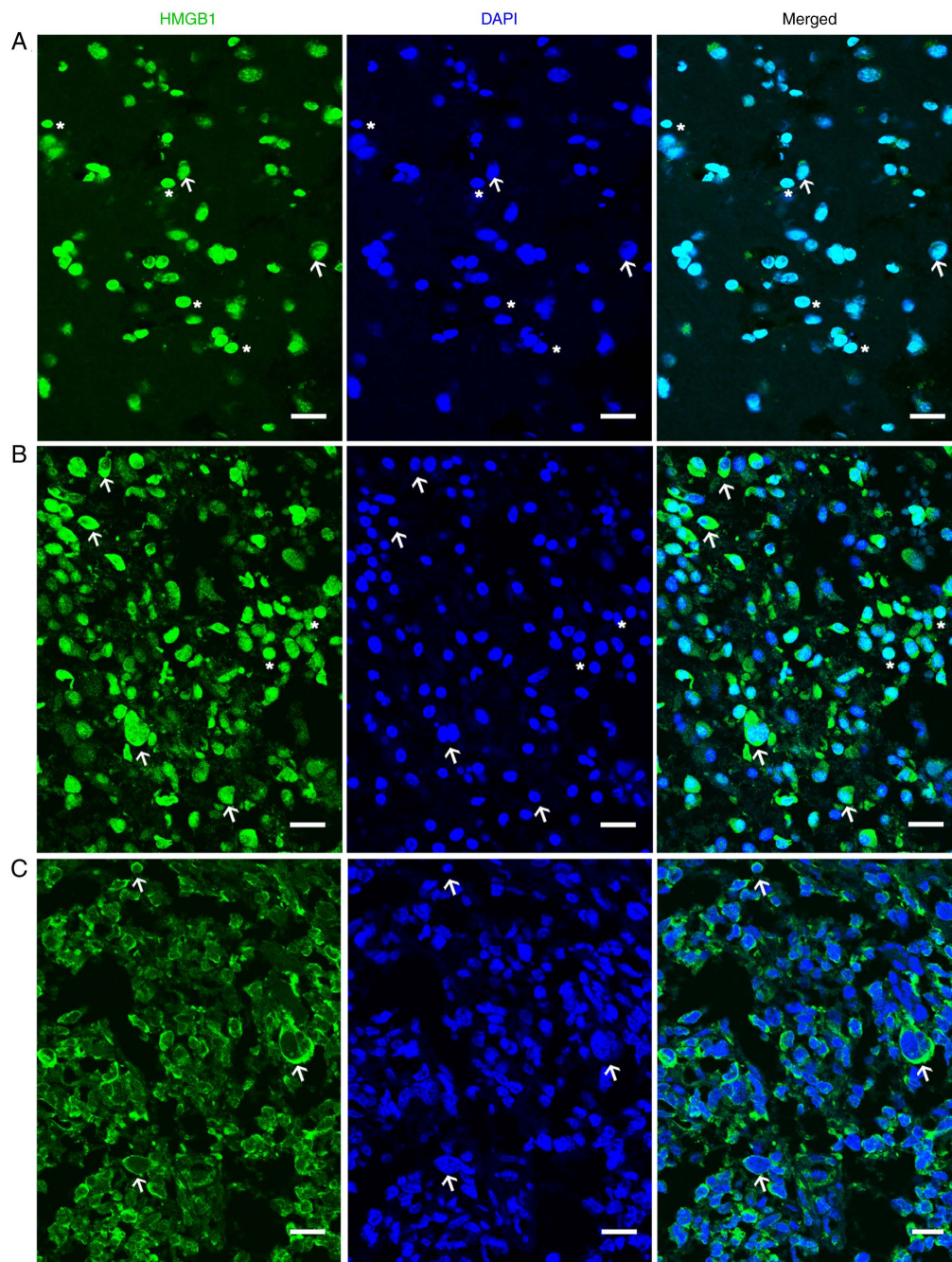


Figure 1. Expression of HMGB1. Expression of HMGB1 in (A) normal tissues and (B) and (C) glioma tissues. Arrows indicate cells with cytoplasmic expression; asterisks indicate nuclear expression. Scale bar, 5  $\mu$ m. HMGB1, high mobility group box 1.

glioma tissues. Considering the limitations in antibody species and reactivity, only the co-localization of HMGB1 with ATP5A (mitochondria), LAMP1 (lysosome), Rab5 (endosome) and GFAP (cytoskeleton) was detected (Fig. 5). The results revealed that HMGB1 and these marker proteins co-localized in glioma tissues.

**Ultrastructural characterization of subcellular localization of HMGB1 in glioma cells.** To gain further insight into the translocation of HMGB1 in glioma cells, HMGB1 localization was examined at the ultrastructural level by performing immunogold electron microscopy on HBSS-treated glioma cells. The results revealed that gold particles were

positioned in the nucleus, cytoplasm and extracellular matrix of the starved glioma cells (Fig. 6A-C), indicating that HMGB1 was released from the nucleus into the cytoplasm and outside of the cell, following starvation stress. In the cytoplasm, gold particles were present within or around the membrane structures. According to the morphological criteria, gold particles were localized within or around the mitochondria (Fig. 6D), ER (Fig. 6E and J), small vesicles (Fig. 6F), endosomes (Fig. 6G), coated vesicles (Fig. 6H) and autolysosomes (Fig. 6I). Furthermore, gold particles were associated with the cytoskeleton (Fig. 6J). Notably, some gold particles were free and did not bind to specific structures in the cytoplasm (Fig. 6K). Collectively, these

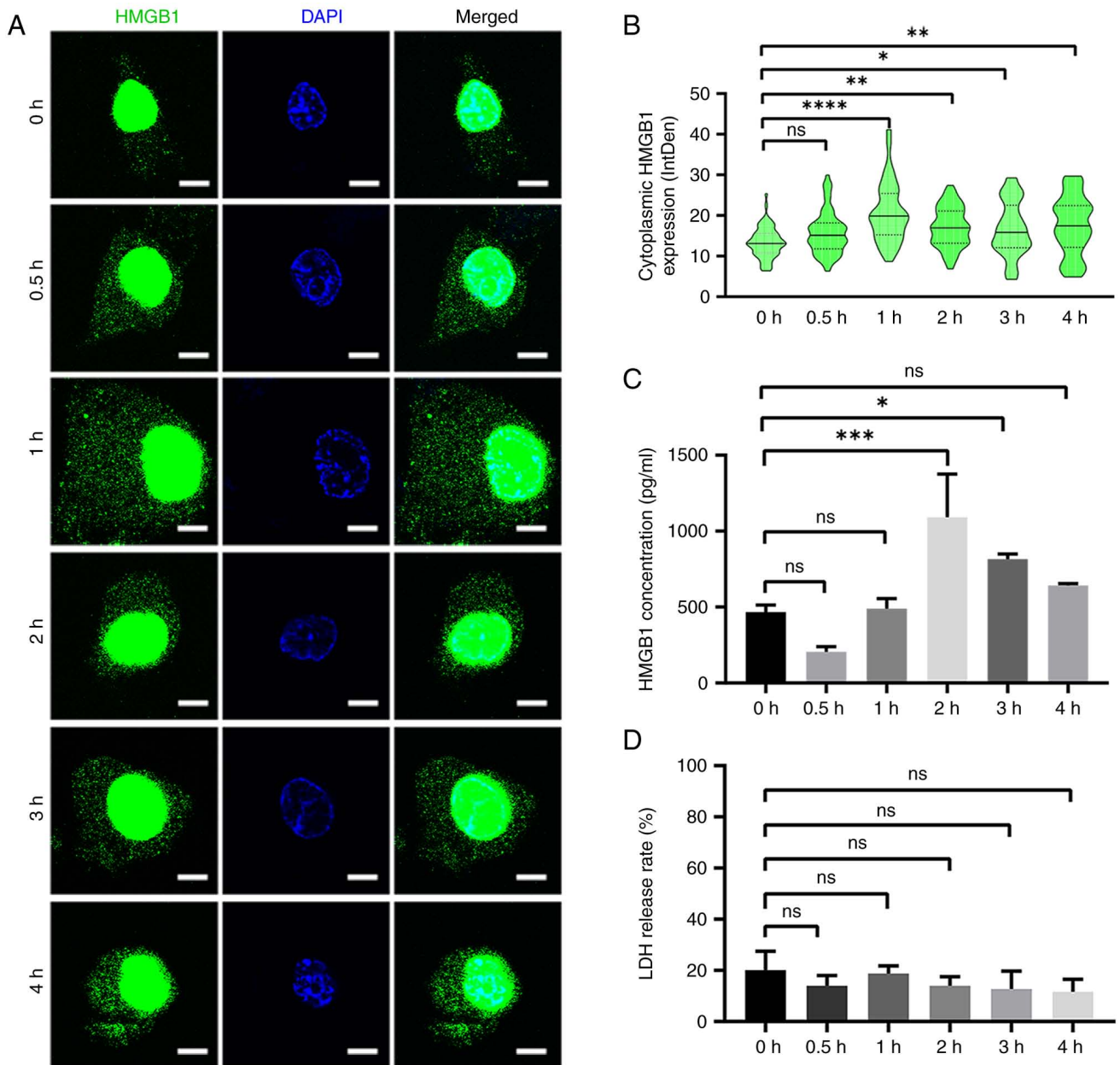


Figure 2. HMGB1 translocation at the indicated time intervals. (A) HMGB1 staining in U87-MG glioma cells at 0, 0.5, 1, 2, 3 and 4 h following starvation with HBSS. Nuclei were stained with 4'6-diamidino-2-phenylindole. Scale bar, 5  $\mu$ m. (B) Cytoplasmic immunoreactivity of HMGB1 at the indicated time intervals was determined (n=3, 16-26 cells per replicate). (C) Supernatants of U87-MG glioma cells treated with HBSS at indicated time intervals were collected, and HMGB1 was detected using ELISA (n=3). (D) The cytotoxicity of HBSS was measured using an LDH release assay (n=3). Data represent the mean  $\pm$  SD; Statistical significance was assessed using one-way ANOVA followed by Tukey's post hoc test. \*P<0.05, \*\*P<0.01, \*\*\*P<0.001 and \*\*\*\*P<0.0001. ns, not significant; HMGB1, high mobility group box 1; HBSS, Hank's balanced salt solution; LDH, lactate dehydrogenase.

experiments revealed that HMGB1 translocated within or around membrane organelles and the cytoskeleton of the starved glioma cells.

**HMGB1 is enriched in membrane-bound compartments.** Subsequently, it was tested whether cytosolic HMGB1 in the starved glioma cells is enclosed in membrane-bound compartments through subcellular fractionation (20,30). Cell lysates of HBSS-treated U87-MG cells were sequentially centrifuged to pellet the nuclei (precipitated along with the cytoskeleton), ER, crude mitochondria and pure mitochondrial pellets, respectively. The pellets were then immunoblotted for the expression of HMGB1 and organelle

markers. Lamin B1,  $\beta$ -actin, CANX and ATP5A were used to label nuclear proteins, cytosolic proteins, ER and mitochondria, respectively.  $\beta$ -actin expression was observed in the nuclei fraction (Fig. 7A). This may be attributed to the nuclei and cytoskeleton precipitating together, and  $\beta$ -actin belonging to the cytoskeletal protein. The results revealed the expression of HMGB1 in both the nuclei and the cytoplasm (Fig. 7A). Moreover, HMGB1 expression was also detected in the ER, crude mitochondria and pure mitochondrial fractions (Fig. 7B), indicating that HMGB1 was enriched in the membrane-bound compartments after starvation.

To further demonstrate the translocation of HMGB1 into membrane-bound compartments, autophagosomes were



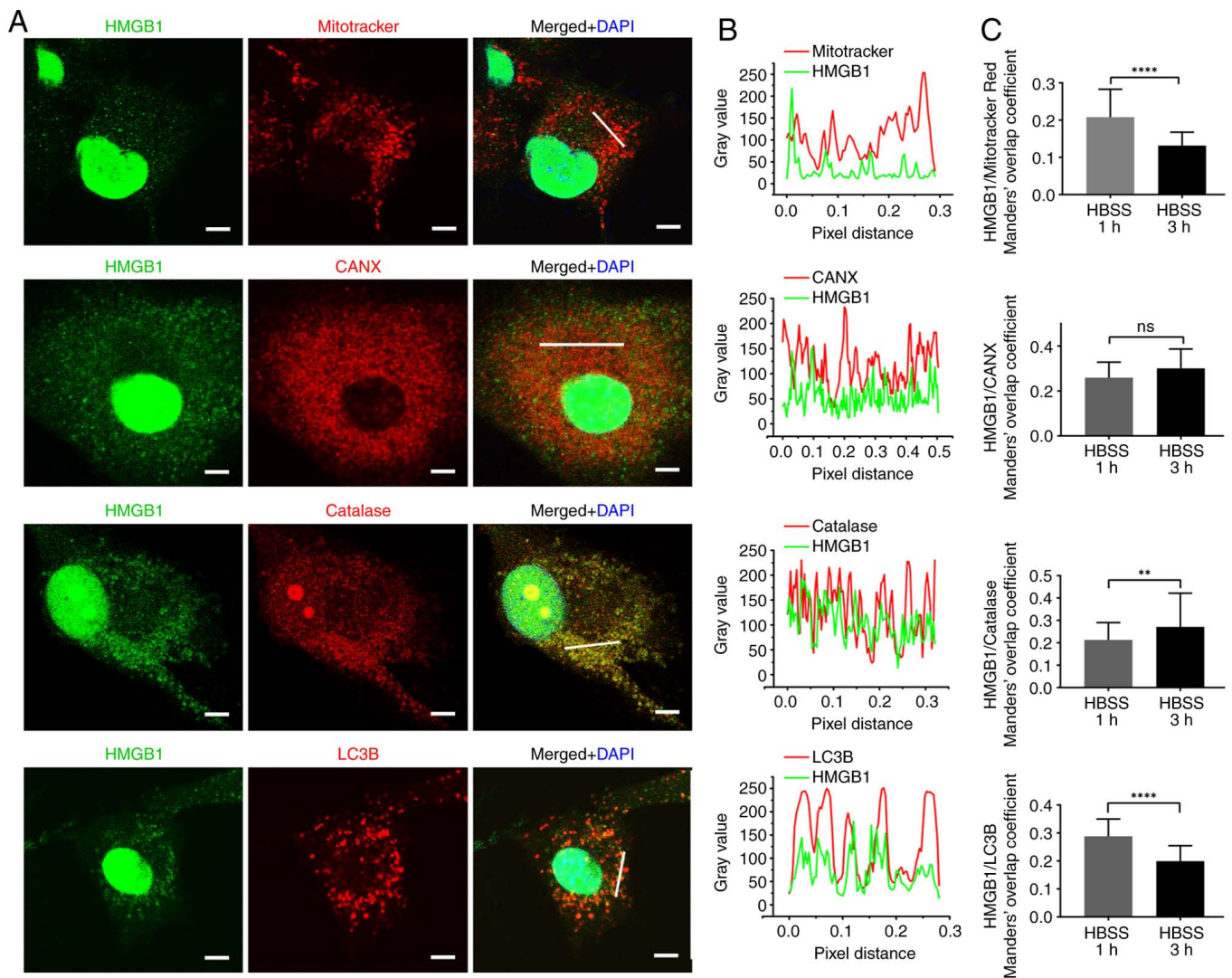


Figure 3. Immunocytochemistry HMGB1 with mitotracker red, CANX, catalase and LC3B. (A) Staining for HMGB1 with mitotracker red probe, CANX, catalase and LC3B antibodies in U87-MG glioma cells at 3 h following HBSS stimulation. Nuclei were stained with 4'6-diamidino-2-phenylindole. Scale bars, 5  $\mu$ m. (B) Line fluorescence tracing from images in (A). (C) Manders' overlap coefficient analysis of HMGB1 and each marker protein 1 and 3 h following HBSS stimulation (n=3, 20-33 cells per replicate). Data represent the mean  $\pm$  SD; an unpaired Student's t-test was used to evaluate statistical significance. \*\*P<0.01 and \*\*\*\*P<0.0001. ns, not significant. HMGB1, high mobility group box 1; CANX, calnexin; LC3B, microtubule-associated proteins 1A/1B light chain 3B; HBSS, Hank's balanced salt solution.

isolated according to a membrane fractionation procedure as previously described (21) (Fig. 7C). Overall, 3, 25 and 100 k membrane pellet fractions were first obtained by applying differential centrifugation to the HBSS-treated U87-MG glioma cells. LC3B-II is enriched in the 25-k fraction (21). WB demonstrated that HMGB1 was enriched in all three fractions, with the 25- and 100-k fractions co-localizing with LC3B-II (Fig. 7D). However, LC3B-I was strongly expressed in the 100-k fraction (Fig. 7D). In general, the ratio of LC3B-II to LC3B-I represents the level of autophagy (31). Therefore, it was considered that autophagosomes were mainly enriched in the 25-k fraction in this experiment. Protease K protection experiments demonstrated that HMGB1 was sequestered in the membrane vesicular structures in the 25- and 100-k fractions (Fig. 7E). Accordingly, these data suggested that HMGB1 translocated to the autophagosomes (25-k fraction) and other types of membrane vesicular structures (100-k fraction) of the starved glioma cells.

*HMGB1 localizes at the MAMs in glioma.* Considering that HMGB1 is dually localized to the mitochondria and ER, the present study then wished to investigate whether HMGB1 localizes to the ER and mitochondria contact sites, termed MAMs. MAMs are highly specialized subcellular compartments located between the mitochondria and ER. They are ER membranes that are in close proximity to the mitochondria, although being biochemically distinct from pure ER and pure mitochondria (32). In the cytoplasm, HMGB1 is distributed non-uniformly and adopts a punctate or patchy distribution, a staining pattern similar to that of MAM-localized proteins (33,34). Herein, firstly, MAMs were examined in glioma cells and tissues. The ER and mitochondria were labeled with CANX and Mitotracker or ATP5A, respectively. The MAMs, the double labeled sites, were calculated through Manders' overlap coefficient. Compared with the HA1800 astrocytes or the normal brain tissues, MAMs were significantly increased

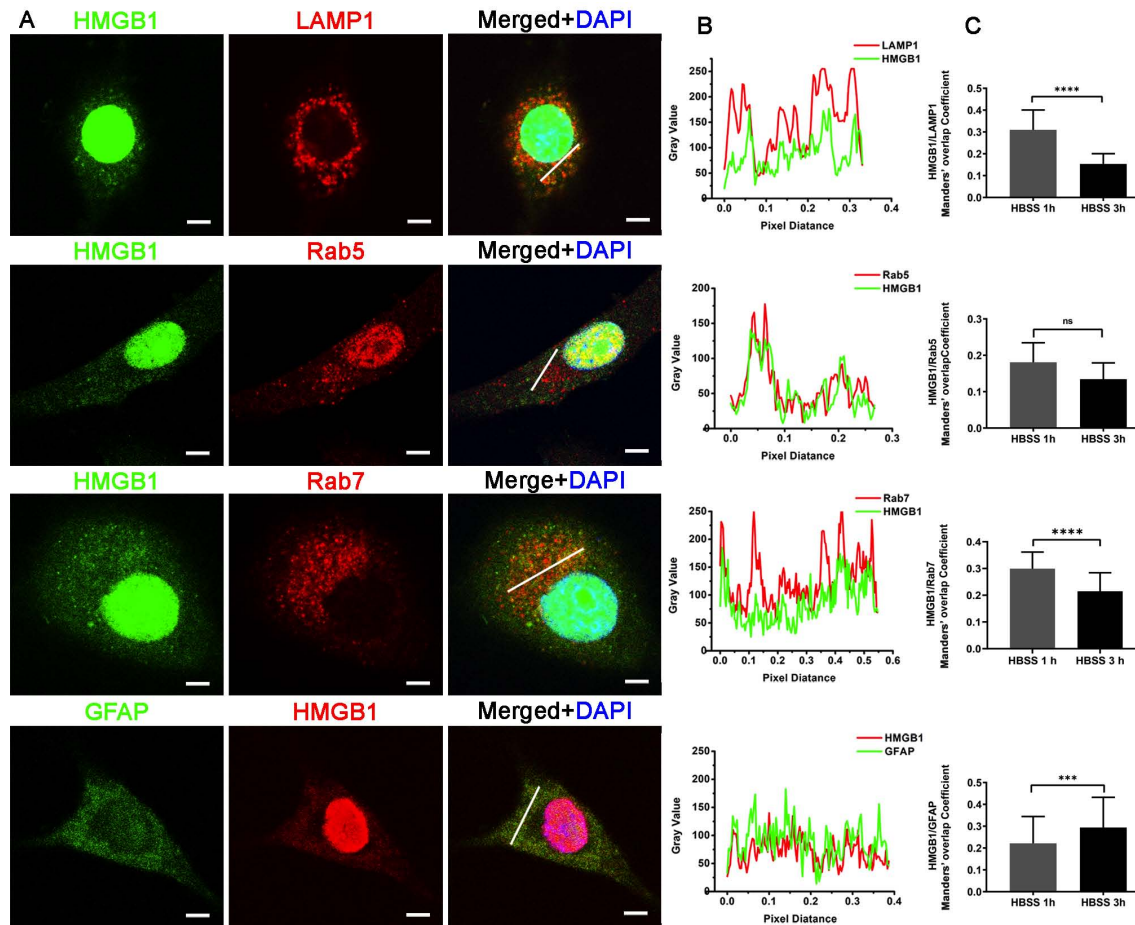


Figure 4. HMGB1 with LAMP1, Rab5, Rab7 and GFAP. (A) Staining for HMGB1 with LAMP1, Rab5, Rab7 and GFAP antibodies in U87-MG glioma cells at 3 h following HBSS stimulation. Nuclei were stained with 4'6-diamidino-2-phenylindole. Scale bars, 5  $\mu$ m. (B) Line fluorescence tracing from images in (A). (C) Manders' overlap coefficient analysis of HMGB1 and each marker protein 1 and 3 h after HBSS stimulation (n=3, 20-33 cells per replicate). Data represent the mean  $\pm$  SD; an unpaired Student's t-test was used to evaluate the statistical significance. \*\*\*\*P<0.0001 and \*\*\*\*P<0.0001. ns, not significant; HMGB1, high mobility group box 1; LAMP1, lysosomal-associated membrane protein 1; GFAP, glial fibrillary acidic protein; HBSS, Hank's balanced salt solution.

in both the glioma cells (Fig. S2A and B) and glioma tissues (Fig. S2C and D). In addition, it was observed that the mitochondria with partial or total cristolysis were in close association with ER profiles establishing MAMs in the transmission electron microscopy images of a case of glioblastoma (Fig. S2E). These results indicated that MAMs were increased in glioma. Subsequently, it was examined whether HMGB1 localized at MAMs through triple ICC staining. The results demonstrated that some HMGB1 puncta were associated with ER and mitochondrial markers in the glioma tissues and HBSS-treated glioma cells (Figs. 8A and B, and S3, as indicated by the arrows). Furthermore, it was examined whether HMGB1 localizes at MAMs by imaging glioma cells (expressing HMGB1-EGFP) in which the mitochondria and ER were labeled with their respective fluorescent probes. The transfection control for the HMGB1 transfection efficiency evaluation was performed through ICC and WB (Figs. S4A and B). The results revealed that HMGB1-EGFP puncta were generally co-localized with both ER and mitochondrial markers (Fig. 8C, as indicated by the arrows). In addition, it was observed that HMGB1 puncta were associated with the MAM marker Sigma1-R (Fig. 8D, as indicated by the arrows). Immunoelectron microscopy further

indicated that HMGB1 gold particles were localized in the narrow cytoplasmic cleft outlining both the mitochondria and expanded ER, thereby confirming that HMGB1 puncta localized at MAMs (Fig. 8E and F). Taken together, these results identified HMGB1 as a novel, to the best of our knowledge, MAM protein in glioma cells following starvation.

*Autophagy contributes to the release of HMGB1 in glioma cells following starvation.* Autophagy positively contributes to HMGB1 secretion via an export pathway in non-tumor cells (35,36). In the present study, HMGB1 translocated to the autophagosomes, lysosomes, endosomes and MAMs [the assembly origin site of autophagosomes (37)], all of which are implicated in autophagy. These results suggest that autophagy mediates the release of HMGB1 from starved glioma cells. As demonstrated in Figs. 9A and B, and S5, the expression of the autophagy marker, LC3B-II, was significantly increased, while that of the autophagy-related protein sequestosome 1 (p62; this protein is incorporated into the autophagosome and then degraded during autophagic process (38-40)), was significantly decreased, indicating an increase in autophagy levels following HBSS treatment. Co-treatment with the early autophagy inhibitor,



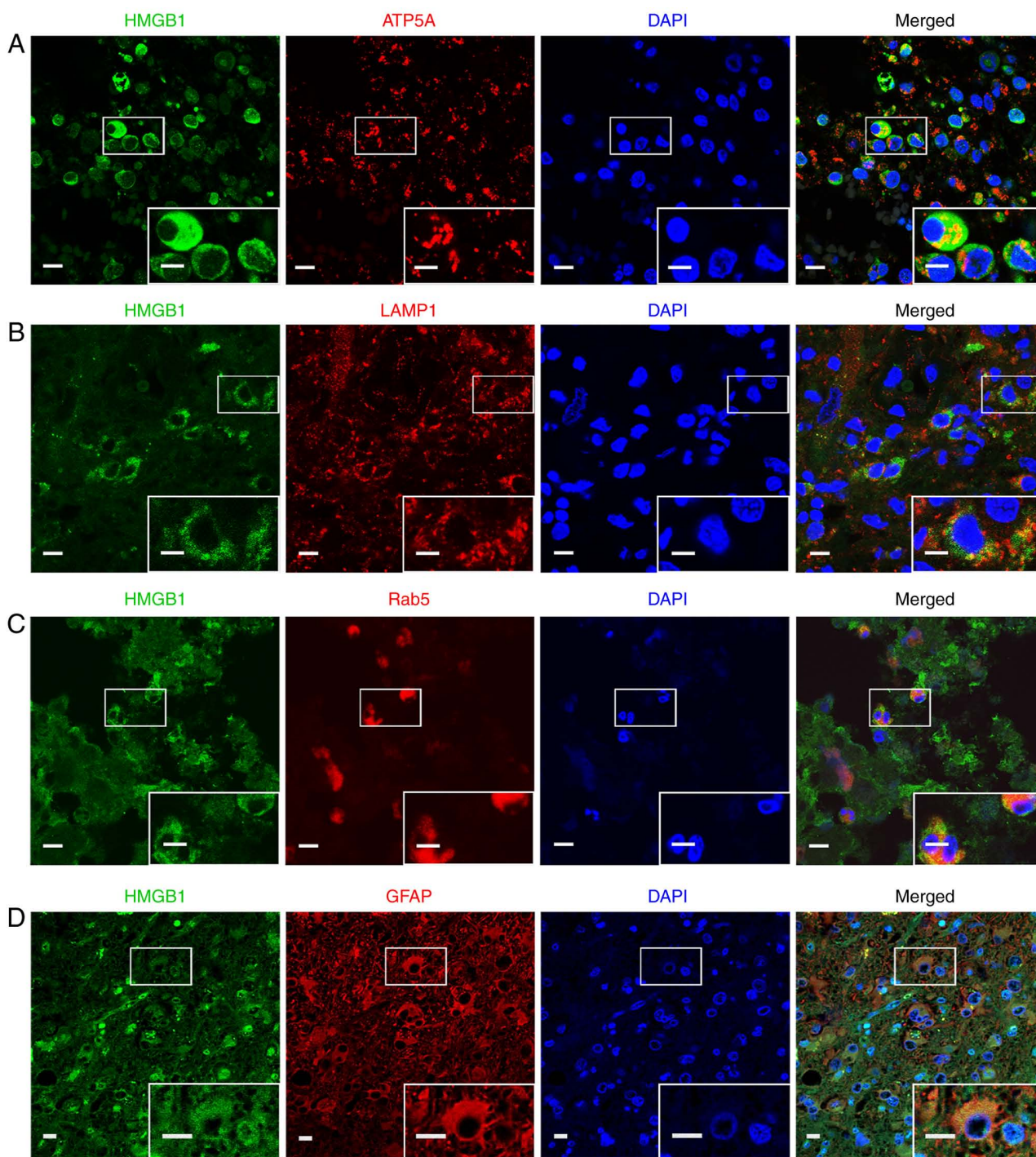


Figure 5. Immunohistochemistry of HMGB1 with (A) ATP5A, (B) LAMP1, (C) Rab5, and (D) GFAP in glioma tissues. Boxed areas in the lower right corner are an enlarged image of the boxed area above. Scale bars in the images with a lower magnification value in (A), (B) and (C) are 10  $\mu$ m, and 5  $\mu$ m in the images with a higher magnification. Scale bars for both the lower and higher magnified images in (D) are 10  $\mu$ m. HMGB1, high mobility group box 1; ATP5A, ATP synthase F1 subunit alpha; LAMP1, lysosomal-associated membrane protein 1; GFAP, glial fibrillary acidic protein.

WOR, decreased the expression of the autophagy marker, LC3B-II. WOR inhibits the initiation of autophagy (41). Considering that CQ inhibits the autophagic flux by decreasing autophagosome-lysosome fusion (42), the accumulation of LC3B-II was observed upon CQ treatment. The results of ELISA demonstrated that HMGB1 secretion was promoted following HBSS treatment; however, the secretion was inhibited after WOR and CQ were applied (Fig. 9C). The results of LDH release and CCK-8 assays revealed that the increased secretion of HMGB1 was not due to

increased non-specific membrane permeability or cell death (Fig. 9D and E). Furthermore, we observed accumulation of HMGB1 containing autophagosomes after the autophagic flux was inhibited by CQ in glioma cells (Fig. 9F-H).

## Discussion

Previous studies have investigated the translocation of HMGB1 to neurons (43), immunocytes (5) and glioma cells (44). These studies clearly revealed the translocation of

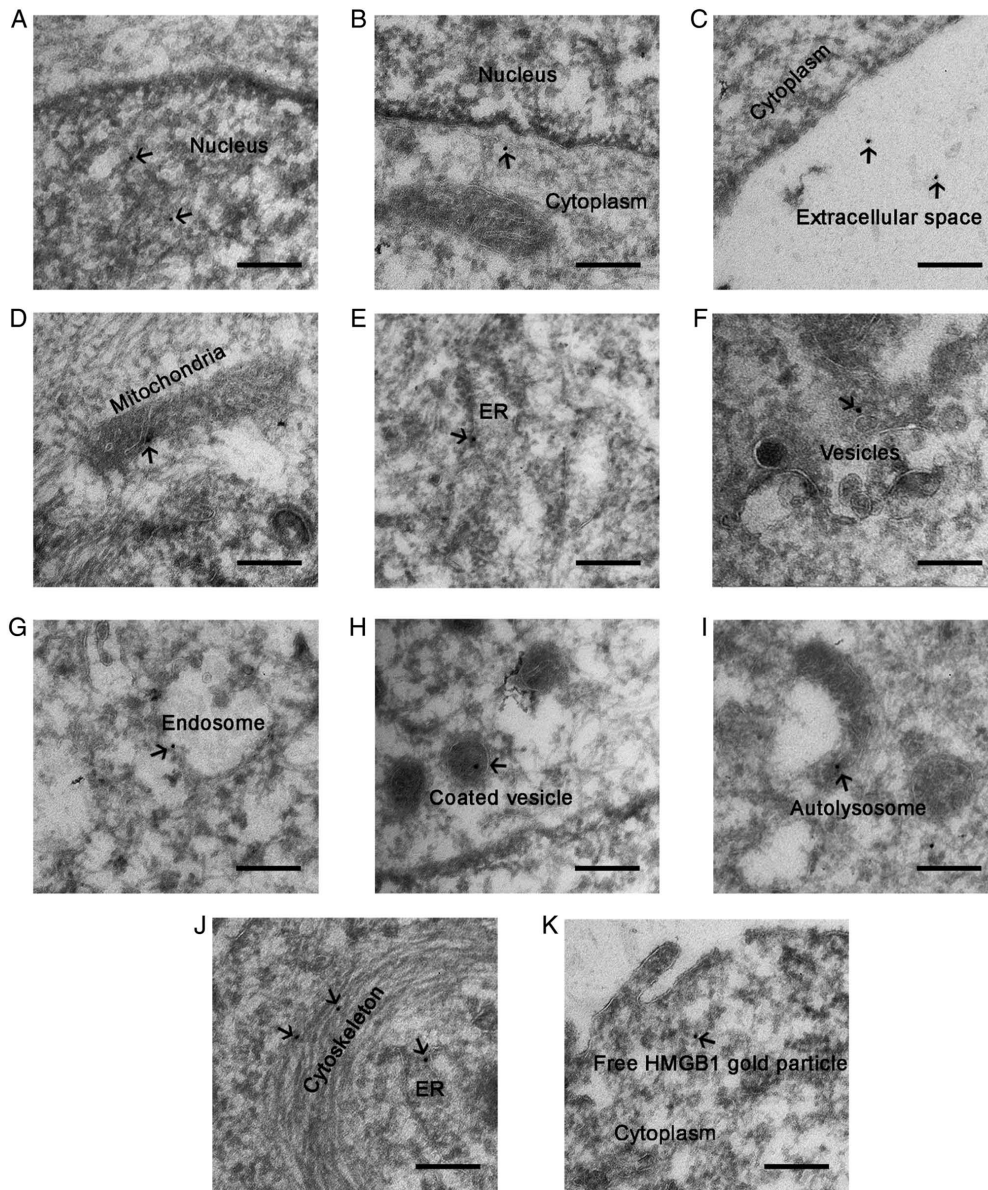


Figure 6. Electron microscopy images of HMGB1 in U87-MG glioma cells treated with HBSS for 3 h. HMGB1 localization was visualized using 10 nm gold particles (indicated by arrows). HMGB1 was localized in the (A) nucleus, (B) cytoplasm, and (C) extracellular space. In the cytoplasm, gold particles were found within or around (D) the mitochondria, (E and J) ER, (F) small vesicles, (G) endosomes, (H) coated vesicles, (I) autolysosomes, and (J) the cytoskeleton. (K) Free gold particles of HMGB1 in the cytoplasm. Scale bar, 200 nm. HMGB1, high mobility group box 1; HBSS, Hank's balanced salt solution; ER, endoplasmic reticulum.

HMGB1 from the nucleus to the extracellular space through cytosolic compartments. Although HMGB1 in the cytoplasm generally exhibits a characteristic granular staining pattern (43,45), information regarding its subcellular localization of HMGB1 in the cytoplasm is limited, particularly in cancer cells (46). In the present study, the translocation of HMGB1 in glioma cells under starvation stress was confirmed. It was observed that HMGB1 was expressed in the nucleus, cytoplasm and extracellular space of the glioma cells. This result is consistent with the tissue array results in a previous study by the authors (44). Similarly, in cultured glioma cells, HMGB1 was released from the nucleus into the cytoplasm and was eventually secreted into the exterior under conditions of starvation. In addition to starvation, it was also observed that  $H_2O_2$ -induced stress caused HMGB1

to translocate from the nucleus to the cytoplasm and locate on the mitochondria (Fig. S1). This result indicates that HMGB1 translocation is common in glioma cells under stress. ICC and immunoelectron microscopy revealed that HMGB1 was imported into the mitochondria, ER, peroxisomes, autophagosomes, lysosomes, early endosomes, late endosomes and the cytoskeleton. In addition, the localization of HMGB1 in these compartments changed with prolonged starvation, indicating a dynamic association between HMGB1 and cytosolic compartments during its release. The release of HMGB1 has been shown to promote tumor growth and metastases through its cytokine, chemokine and growth factor activities, whereas cytoplasmic HMGB1 increases chemoresistance due to its pro-autophagic activity (47,48). HMGB1 cannot enter the ER for processing as there is no signaling peptide

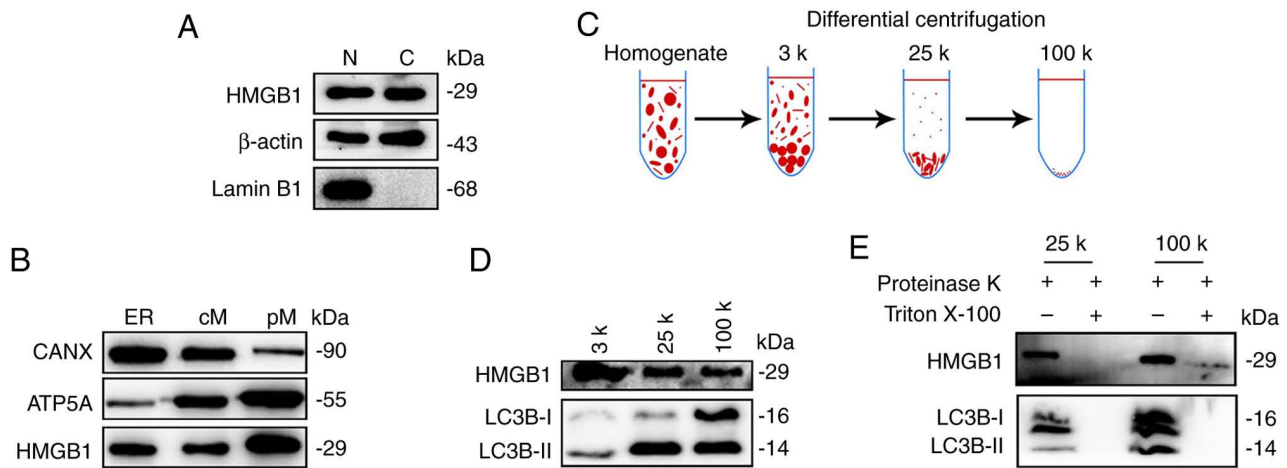


Figure 7. HMGB1 is enriched in membrane-bound compartments. (A) Pellets containing nuclei and cytoskeletons (N) and cytoplasmic proteins (C) were collected from the HBSS-treated U87-MG glioma cells and immunoprobed with Lamin B1 (marker for the nuclear proteins),  $\beta$ -actin (marker for the cytosolic proteins) and HMGB1. (B) Pellets containing ER, cM and pM were fractionated and immunoprobed with HMGB1, the ER marker, CANX, and the mitochondria marker, ATP5A. HMGB1 was detected in the membrane-bound compartments. (C) Membrane fractionation scheme. Briefly, U87-MG cells were starved in HBSS for 1 h, collected and then homogenized. Cell lysates were differentially centrifuged at 3,000 x g, 25,000 x g, and 100,000 x g at RT. (D) The expression levels of LC3B and HMGB1 in different fractionations were measured using western blotting. (E) Proteinase K digestion was performed using the 25-k and 100-k membrane fractions. HMGB1, high mobility group box 1; HBSS, Hank's balanced salt solution; ER, endoplasmic reticulum; cM, crude mitochondria; pM, pure mitochondria; CANX, calnexin; ATP5A, ATP synthase F1 subunit alpha; LC3B, microtubule-associated proteins 1A/1B light chain 3B.

enabling this action; that is, HMGB1 is rather secreted via an endosome-lysosome or autophagy-mediated non-canonical pathway and not extracellularly via the classical ER-Golgi secretion pathway (36,49). HMGB1 co-localizes with the lysosomal marker protein, LAMP1, suggesting that HMGB1 may be secreted into the extracellular matrix from lysosomes or endosome-lysosomes (50). Different cell types release HMGB1 via different mechanisms. In monocytes, HMGB1 is first translocated from the nucleus to the cytoplasm and is then encapsulated in secretory lysosomes or other membrane organelles. These membrane structures then fuse with the cell membrane to release HMGB1 (50). Kim *et al* (36) reported that early autophagy and late endosomes mediate the exocrine pathway of HMGB1 in 293T cells, human monocyte THP-1 cells, and mouse embryonic fibroblasts. In psoriatic keratinocytes, early and late autophagy play pivotal roles in the extracellular secretion of HMGB1 (35).

Understanding the HMGB1 secretory pathway is crucial, since extracellular HMGB1 has pro-inflammatory functions and serves as a multifunctional alarm to regulate cell proliferation, tissue remodeling and tumor progression (36). In the present study, treatment with WOR, which inhibits the initiation of autophagy (41) and CQ, which reduces autophagosome-lysosome fusion (42), prevent the extracellular secretion of HMGB1, supporting that HMGB1 secretion was mediated by early and late autophagy in glioma cells under starvation stress. Elmaci *et al* (51) reported that HMGB1 was secreted into the extracellular space via autophagy in dying glioma cells. The data of the present study demonstrated the translocation of HMGB1 to subcellular compartments during its release; cytosolic HMGB1 in glioma cells can be imported into or around autophagosomes, endosomes, lysosomes and MAMs. Endosomes, particularly late endosomes, are destined to evolve into lysosomes (52). MAMs mark the initiation sites of autophagosome formation (37). Thus, all these cellular

compartments are involved in autophagy. Additionally, the autophagy-lysosomal pathway may mediate the selective release of HMGB1 in glioma cells under nutrient-poor conditions, which do not induce cell death or non-specific membrane permeability.

In addition to the autophagy-related cellular compartments, HMGB1 translocation inside the lumen of the mitochondria and ER was observed, as well as in the peroxisomes and cytoskeleton. Previous studies have examined the localization of HMGB1 in the mitochondria, demonstrating also that HMGB1 translocation to the mitochondria may affect mitochondrial morphology, energy metabolism, and autophagy (53). In addition, HMGB1 has a high affinity to mitochondrial DNA (mtDNA) released from injured hepatocellular carcinoma cells (54). Thus, HMGB1 localization in the mitochondria may be associated with remodeling of morphology and energy metabolism, as well as mtDNA release following starvation. Moreover, HMGB1 was localized in decomposed mitochondria engulfed by autolysosomes (Fig. 6I), suggesting that HMGB1 may mediate mitophagy in starved glioma cells. In addition, hyperoxic conditions increase the generation of mitochondrial reactive oxygen species and the overexpression and secretion of HMGB1 in the brain and lungs, indicating a potential association between mitochondrial dysfunction and HMGB1 translocation (53). HMGB1 lacks leader peptides and thus cannot enter the conventional ER-to-Golgi secretory pathway (36). However, herein, immunoelectron microscopy demonstrated that HMGB1 particles were localized in the ER lumen (Fig. 6E and J). Previous studies have revealed that HMGB1 plays an essential role in ER stress (55,56). However, the association between HMGB1 and the ER in gliomas requires further elucidation in future studies. Wang *et al* (43) demonstrated that HMGB1 can be imported into the peroxisomes of ischemic neurons. In the present study, HMGB1 and the



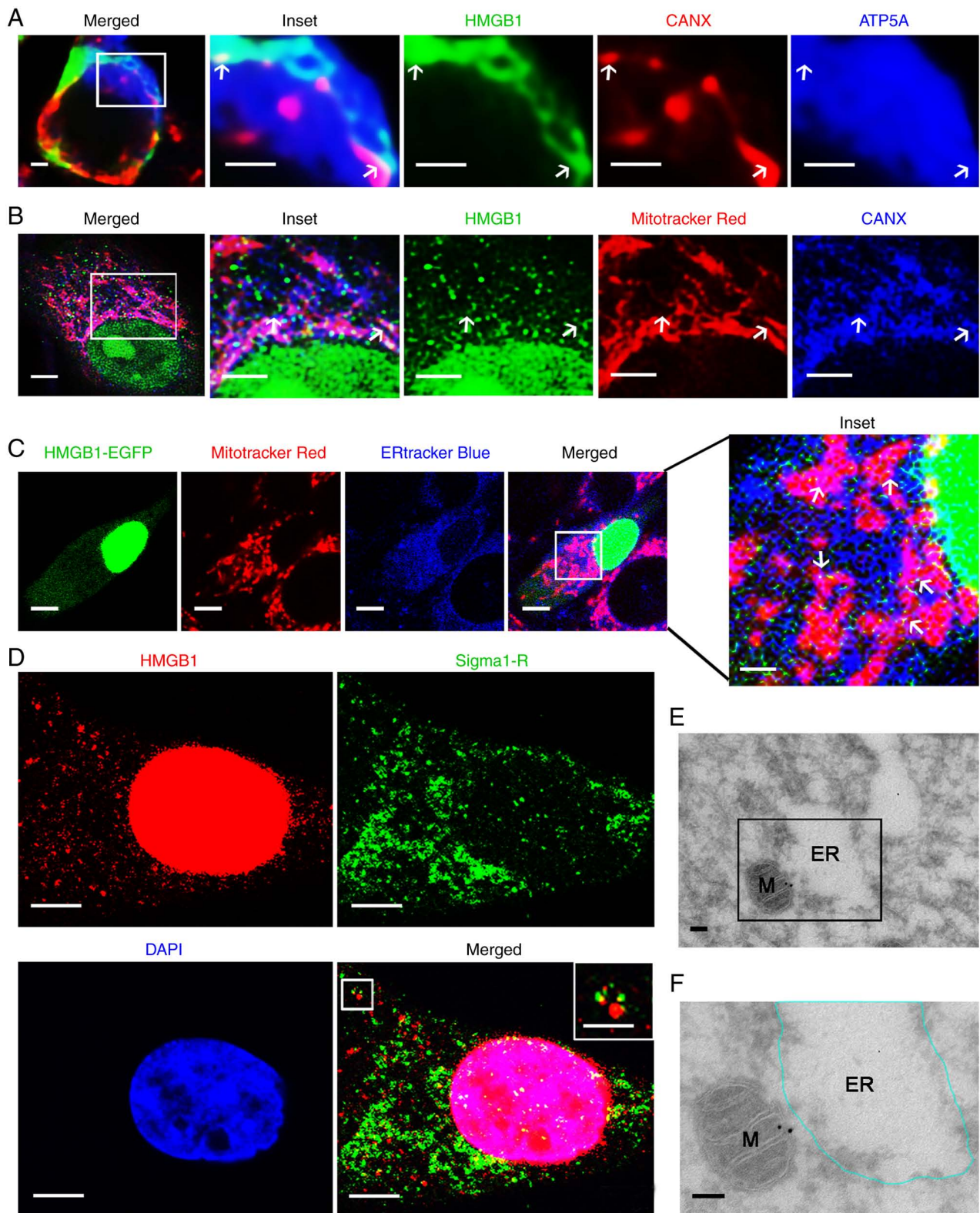


Figure 8. HMGB1 is localized at MAMs in glioma. (A) Paraffin-embedded glioma sections were co-stained for HMGB1 and the ER marker, CANX, as well as the mitochondrial protein, ATP5A. HMGB1 was detected at MAMs, as indicated by arrows. The 'inset' image is an enlarged image of the boxed region in the merged image. (B) HBSS-treated U87-MG cells were co-stained for HMGB1, CANX and Mitotracker Red. Arrows indicate the localization of HMGB1 at MAMs. The 'inset' image is an enlarged image of the boxed region in the merged image. (C) U87-MG cells were transfected with the HMGB1-EGFP plasmid and then treated with HBSS. ER and mitochondria were labeled with ERtracker Blue and Mitotracker Red, respectively. The 'inset' image is an enlarged image of the boxed region in the merged image. White arrows indicate the localization of HMGB1 in MAMs. (D) HBSS-treated U87-MG cells were co-stained for HMGB1 and Sigma1-R. The boxed area in the upper right corner is an enlarged image of the boxed area on the upper left corner. (E) Representative images of HBSS-treated U87-MG cells showing the localization of HMGB1 by immune gold. The boxed area and expanded ER are amplified and outlined, respectively, in (F). M, mitochondria. Scale bars: (A) 1  $\mu$ m, (B) lower magnified image 3  $\mu$ m and higher magnified images 2  $\mu$ m, (C) lower magnified images 5  $\mu$ m and higher magnified image 1  $\mu$ m, (D) 2  $\mu$ m, and inset image 1  $\mu$ m, (E and F) 100 nm. HMGB1, high mobility group box 1; MAMs, mitochondria-associated endoplasmic reticulum membranes; ER, endoplasmic reticulum; CANX, calnexin; ATP5A, ATP synthase F1 subunit alpha; HBSS, Hank's balanced salt solution; Sigma1-R, sigma 1 receptor.

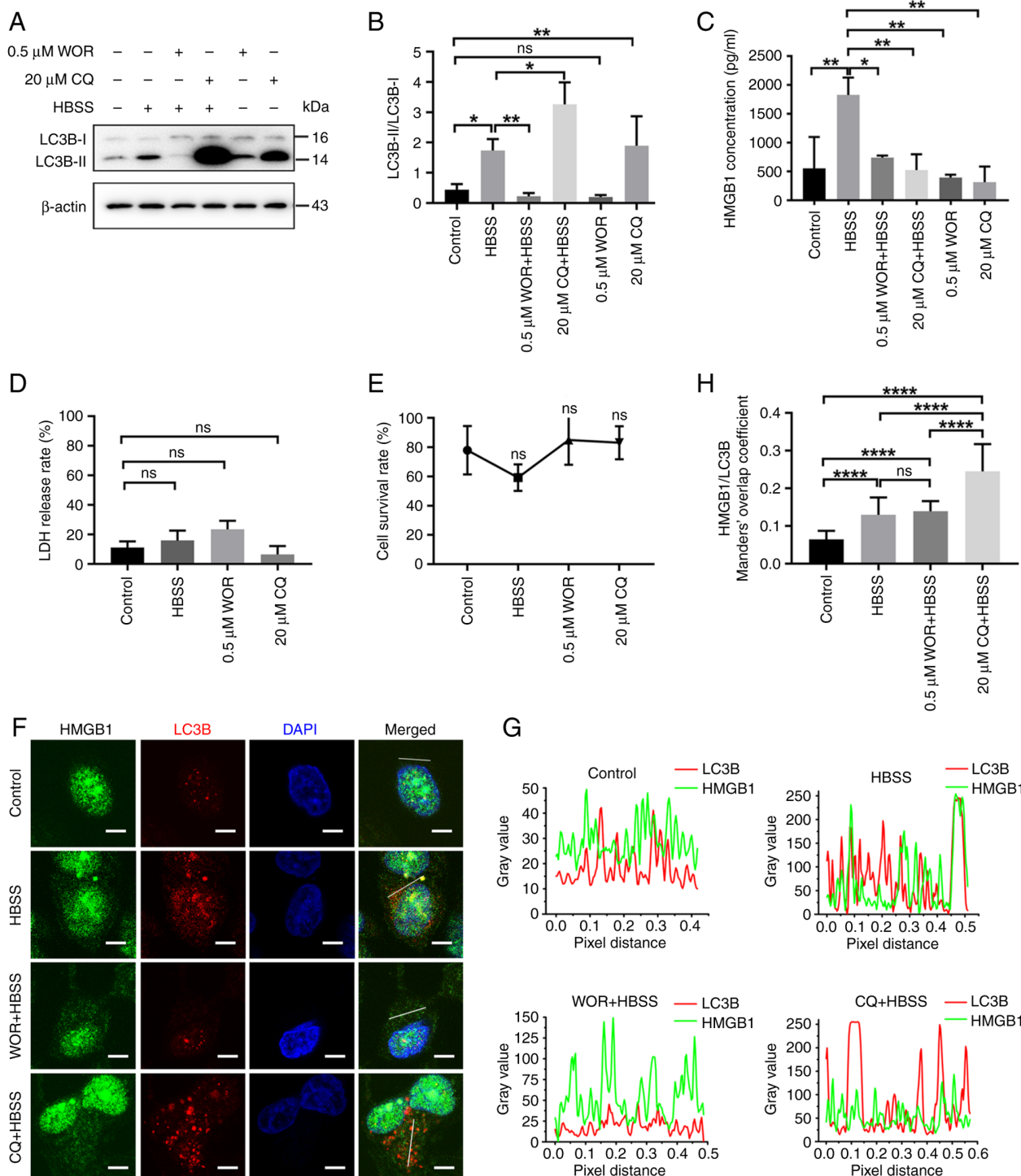


Figure 9. HMGB1 secretion is regulated by autophagy-mediated secretion in glioma cells. (A) U251 glioma cells were pretreated with 0.5  $\mu$ M WOR and 20  $\mu$ M CQ for 2 h and then treated with HBSS for 3 h. Whole cell lysates immunoblotted with anti-LC3B and anti- $\beta$ -actin antibodies. (B) Statistical analysis of LC3B-II/LC3B-I ratio (n=3). (C) U251 glioma cells were treated with 0.5  $\mu$ M WOR and 20  $\mu$ M CQ for 2 h and then treated with HBSS for 3 h. The secreted HMGB1 levels were measured using ELISA (n=3). (D) LDH release assay determined the cytotoxicity of HBSS, 0.5  $\mu$ M WOR and 20  $\mu$ M CQ (n=3). (E) Treatment with HBSS (3 h), WOR (3 h, 0.5  $\mu$ M), or CQ (3 h, 20  $\mu$ M) did not induce the apoptosis of U251 glioma cells, as determined using CCK-8 assay (n=3). (F) U251 glioma cells were treated with 0.5  $\mu$ M WOR and 20  $\mu$ M CQ for 2 h and then treated with HBSS for 3 h. Immunostaining of HMGB1 and the autophagosome marker, LC3B, in U251 glioma cells subjected to different treatments. (G) Line fluorescence tracing from images in (F). (H) Manders' overlap coefficient analysis of HMGB1 and LC3B (n=3, 10-15 cells per replicate). Data represent the mean  $\pm$  SD; one-way ANOVA followed by Tukey's post-hoc test was used to evaluate statistical significance. \*P<0.05, \*\*P<0.01 and \*\*\*\*P<0.0001. ns, not significant. HMGB1, high mobility group box 1; WOR, wortmannin; CQ, chloroquine; HBSS, Hank's balanced salt solution; LC3B, microtubule-associated proteins 1A/1B light chain 3B; LDH, Lactate dehydrogenase; CCK-8, Cell Counting Kit-8.

peroxisome marker protein catalase co-localized in glioma cells. Catalase is an H<sub>2</sub>O<sub>2</sub>-degrading enzyme. In addition,

other redox-related enzymes can also be detected in peroxisomes. Therefore, it was hypothesized that peroxisomes



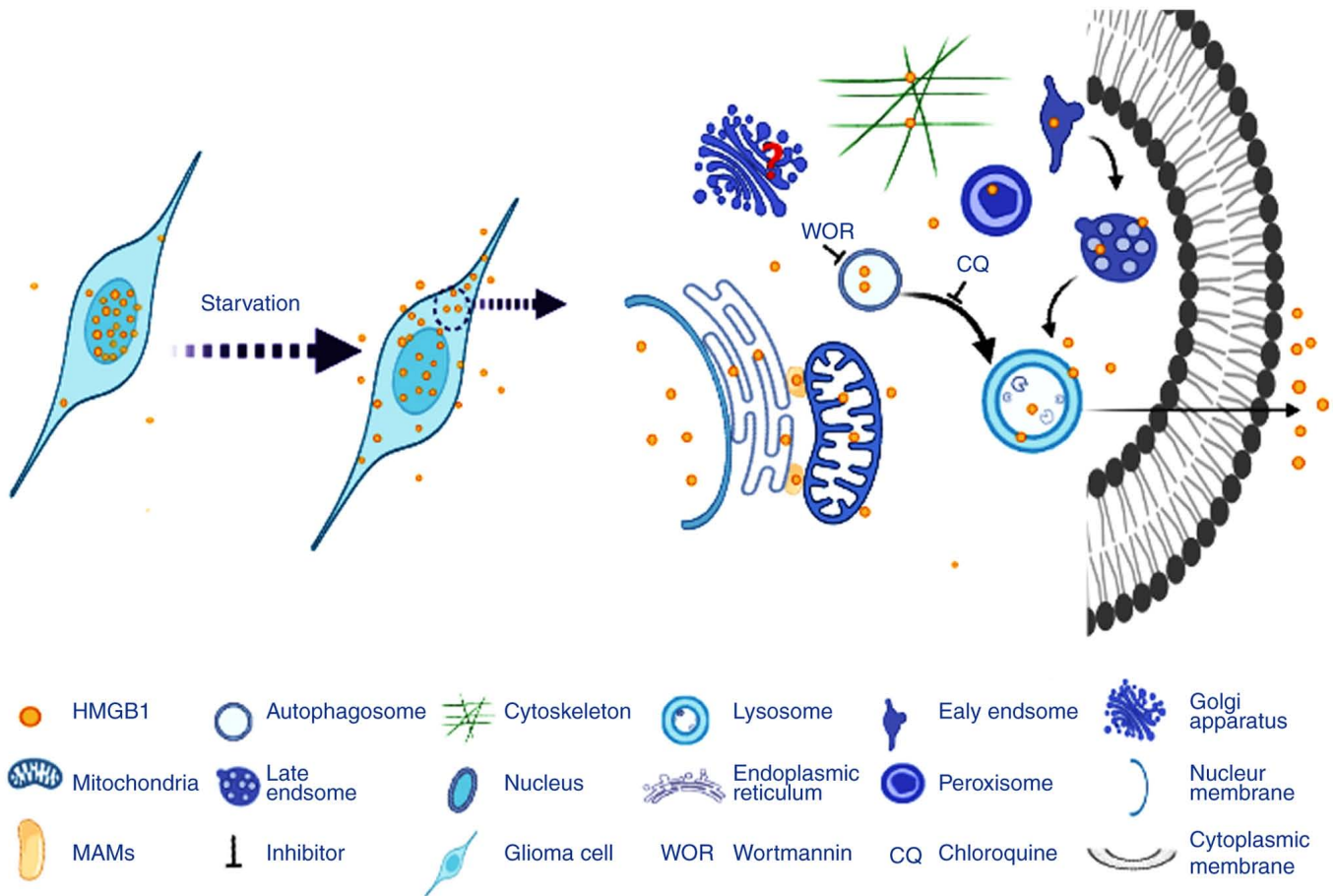


Figure 10. Schematic diagram demonstrating the subcellular localization of HMGB1 in glioma cells. Starvation stress triggers the translocation of HMGB1 from the nucleus to the cytoplasm and the extracellular milieu. In the cytoplasm, HMGB1 can be imported into the mitochondria, ER, MAMs, peroxisomes, autophagosomes, lysosomes, early endosomes, late endosomes and cytoskeleton. Early (inhibited by WOR) and late autophagy (inhibited by CQ) mediated the extracellular secretion of HMGB1. HMGB1, high mobility group box 1; ER, endoplasmic reticulum; MAMs, mitochondria-associated endoplasmic reticulum membranes; WOR, wortmannin; CQ, chloroquine.

are involved in the regulation of the redox state and related intracellular signaling pathways (57,58). In addition, HMGB1 co-localized with GFAP, and the Manders' overlap coefficient between them increased with the release of HMGB1. GFAP is a well-known marker protein for astrocytes and an intermediate filament. Previous studies have reported the co-localization of HMGB1 and GFAP (25,59). The cytoskeleton tracks vesicular trafficking, and aberrant vesicular trafficking and cytoskeletal interactions have been observed in cancer cells (60). Accordingly, it was hypothesized that the cytoskeleton is required for vesicular trafficking and extracellular secretion of HMGB1 in glioma cells under conditions of starvation.

The present study has some limitations. For example, it was not investigated whether HMGB1 is transported to the Golgi apparatus. Immunoelectron microscopy with gold particles of different sizes is suitable for precisely distinguishing between organelles. In addition, ascorbate peroxidase-based proximity labeling technique can be used to image HMGB1 profiles in subcellular compartments using electron microscopy (61,62). Several functional factors, including Golgi reassembly stacking protein 2, ADP ribosylation factor 1 and secretion-associated Ras-related GTPase 1A, are required for secretory autophagy (36). The Ras-related proteins RAB8a, RAB11a

and RAB27a regulate polarized membrane trafficking and plasma membrane fusion (63-65). Furthermore, vesicle-associated membrane protein 7, synaptotagmin-7, or altering the dynamics of lysosomes by inhibiting ADP ribosylation factor like GTPase 8B, could prevent lysosome exocytosis (66-68). Therefore, knockdown or overexpression experiments are necessary to verify the functions of these factors in HMGB1 secretion. The present study was conducted primarily *in vitro*. *In vivo* experiments also need to be conducted to complete the entire study design.

In conclusion, the present study demonstrated that starvation-induced stress induced the translocation of HMGB1 from the nucleus to the cytoplasm and extracellular space in glioma cells. In the cytoplasm, HMGB1 was transported to various cellular compartments, including the mitochondria, ER, MAMs, peroxisomes, autophagosomes, early endosomes, late endosomes, lysosomes and cytoskeleton. Early and late autophagy may be involved in the extracellular secretion of HMGB1 from glioma cells under the same conditions (Fig. 10). Extracellular HMGB1 is a risk factor for several malignancies. The aforementioned results contribute to the further understanding of the translocation and secretion pathways of HMGB1, which may provide a novel perspective for designing inhibitors of HMGB1 secretion for the treatment of glioma.



## Acknowledgements

The authors would like to thank Dr Xia Chu from the Department of Histology at the 988th Hospital of the Joint Logistic Support Force (Zhengzhou, China) for providing the tissue sections, and Dr Ying Li from the Biomedical Testing Center of Tsinghua University (Beijing, China) for providing technical assistance.

## Funding

The present study was supported by the National Natural Science Foundation of China (grant no. 81402455), China Postdoctoral Science Foundation (grant no. 2019M653946) the Cultivation Fund of Zhengzhou University in 2021 (grant no. JC21835040) and the opening project of State Key Laboratory of Explosion Science and Technology (Beijing Institute of Technology) (grant no. KFJJ23-09M).

## Availability of data and materials

The datasets used and/or analyzed during the current study are available from the corresponding author on reasonable request.

## Authors' contributions

All authors (XC, AY and LJ) contributed to the conception and design of this study. Material preparation, data collection and analyses were performed by XC and AY. The first draft of the manuscript was written by LJ, and all authors commented on previous versions of the manuscript. All authors confirm the authenticity of the raw data and have read and approved the final version of the manuscript.

## Ethics approval and consent to participate

The present study was performed in accordance with the principles of the Declaration of Helsinki. Approval was granted by the Ethics Committees of 988th Hospital of the Joint Logistic Support Force (Zhengzhou, China). Written informed consent was obtained from all the participants.

## Patient consent for publication

Not applicable.

## Competing interests

The authors declare that they have no competing interests.

## References

- Perry A and Wesseling P: Histologic classification of gliomas. *Handb Clin Neurol* 134: 71-95, 2016.
- Xu S, Tang L, Li X, Fan F and Liu Z: Immunotherapy for glioma: Current management and future application. *Cancer Lett* 476: 1-12, 2020.
- Louis DN, Perry A, Reifenberger G, von Deimling A, Figarella-Branger D, Cavenee WK, Ohgaki H, Wiestler OD, Kleihues P and Ellison DW: The 2016 World Health Organization Classification of Tumors of the central nervous system: A summary. *Acta Neuropathol* 131: 803-820, 2016.
- Mendonça Gorgulho C, Murthy P, Liotta L, Espina V and Lotze MT: Different measures of HMGB1 location in cancer immunology. *Methods Enzymol* 629: 195-217, 2019.
- Le Y, Wang Y, Zhou L, Xiong J, Tian J, Yang X, Gai X and Sun Y: Cigarette smoke-induced HMGB1 translocation and release contribute to migration and NF- $\kappa$ B activation through inducing autophagy in lung macrophages. *J Cell Mol Med* 24: 1319-1331, 2020.
- Wang S and Zhang Y: HMGB1 in inflammation and cancer. *J Hematol Oncol* 13: 116, 2020.
- Völz K, Brezniceanu ML, Böscher S, Brabletz T, Kirchner T, Göttel D, Joos S and Zörnig M: Increased expression of high mobility group box 1 (HMGB1) is associated with an elevated level of the antiapoptotic c-IAP2 protein in human colon carcinomas. *Gut* 55: 234-242, 2006.
- Akaike H, Kono K, Sugai H, Takahashi A, Mimura K, Kawaguchi Y and Fujii H: Expression of high mobility group box chromosomal protein-1 (HMGB-1) in gastric cancer. *Anticancer Res* 27: 449-457, 2007.
- Ranganathan A, Gunnarsson O and Casarett D: Palliative care and advance care planning for patients with advanced malignancies. *Ann Palliat Med* 3: 144-149, 2014.
- Seidu RA, Wu M, Su Z and Xu H: Paradoxical role of high mobility group box 1 in glioma: A suppressor or a promoter? *Oncol Rev* 11: 325, 2017.
- Xue J, Suarez JS, Minaai M, Li S, Gaudino G, Pass HI, Carbone M and Yang H: HMGB1 as a therapeutic target in disease. *J Cell Physiol* 236: 3406-3419, 2021.
- Zhao M, Zhang Y, Jiang Y, Wang K, Wang X, Zhou D, Wang Y, Yu R and Zhou X: YAP promotes autophagy and progression of gliomas via upregulating HMGB1. *J Exp Clin Cancer Res* 40: 99, 2021.
- Wang XJ, Zhou SL, Fu XD, Zhang YY, Liang B, Shou JX, Wang JY and Ma J: Clinical and prognostic significance of high-mobility group box-1 in human gliomas. *Exp Ther Med* 9: 513-518, 2015.
- Gao XY, Zang J, Zheng MH, Zhang YF, Yue KY, Cao XL, Cao Y, Li XX, Han H, Jiang XF and Liang L: Temozolomide treatment induces HMGB1 to promote the formation of glioma stem cells via the TLR2/NEAT1/Wnt pathway in glioblastoma. *Front Cell Dev Biol* 9: 620883, 2021.
- Li Z, Fu WJ, Chen XQ, Wang S, Deng RS, Tang XP, Yang KD, Niu Q, Zhou H, Li QR, *et al*: Autophagy-based unconventional secretion of HMGB1 in glioblastoma promotes chemosensitivity to temozolomide through macrophage M1-like polarization. *J Exp Clin Cancer Res* 41: 74, 2022.
- Grasman G, Smolle E, Olschewski H and Leithner K: Gluconeogenesis in cancer cells-repurposing of a starvation-induced metabolic pathway? *Biochim Biophys Acta Rev Cancer* 1872: 24-36, 2019.
- Finicle BT, Jayashankar V and Edinger AL: Nutrient scavenging in cancer. *Nat Rev Cancer* 18: 619-633, 2018.
- Komori T: The 2016 WHO classification of tumours of the central nervous system: The major points of revision. *Neurol Med Chir (Tokyo)* 57: 301-311, 2017.
- Fan W, Song Y, Ren Z, Cheng X, Li P, Song H and Jia L: Glioma cells are resistant to inflammation-induced alterations of mitochondrial dynamics. *Int J Oncol* 57: 1293-1306, 2020.
- Prajapati P, Wang WX, Nelson PT and Springer JE: Methodology for subcellular fractionation and MicroRNA examination of mitochondria, mitochondria associated ER membrane (MAM), ER, and cytosol from human brain. *Methods Mol Biol* 2063: 139-154, 2020.
- Zhang M, Kenny SJ, Ge L, Xu K and Schekman R: Translocation of interleukin-1 $\beta$  into a vesicle intermediate in autophagy-mediated secretion. *Elife* 4: e11205, 2015.
- Penjweini R, Deville S, Haji Maghsoudi O, Notelaers K, Ethirajan A and Ameloot M: Investigating the effect of poly-L-lactic acid nanoparticles carrying hypericin on the flow-biased diffusive motion of HeLa cell organelles. *J Pharm Pharmacol* 71: 104-116, 2019.
- Suwanakul N, Midorikawa K, Du C, Qi YP, Zhang J, Xiang BD, Murata M and Ma N: Subcellular localization of HMGB1 in human cholangiocarcinoma: Correlation with tumor stage. *Discov Oncol* 12: 49, 2021.
- Satoh TK: The role of HMGB1 in inflammatory skin diseases. *J Dermatol Sci* 107: 58-64, 2022.
- Wang X, Zhou W, Li X, Ren J, Ji G, Du J, Tian W, Liu Q and Hao A: Graphene oxide suppresses the growth and malignancy of glioblastoma stem cell-like spheroids via epigenetic mechanisms. *J Transl Med* 18: 200, 2020.

26. van Asperen JV, Robe PAJT and Hol EM: GFAP alternative splicing and the relevance for disease—a focus on diffuse gliomas. *ASN Neuro* 14: 17590914221102065, 2022.
27. Uceda-Castro R, van Asperen JV, Vennin C, Sluijs JA, van Bodegraven EJ, Margarido AS, Robe PAJ, van Rheenen J and Hol EM: GFAP splice variants fine-tune glioma cell invasion and tumour dynamics by modulating migration persistence. *Sci Rep* 12: 424, 2022.
28. Pastorek L, Sobol M and Hozák P: Colocalization coefficients evaluating the distribution of molecular targets in microscopy methods based on pointed patterns. *Histochem Cell Biol* 146: 391-406, 2016.
29. Khushi M, Napier CE, Smyth CM, Reddel RR and Arthur JW: MatCol: A tool to measure fluorescence signal colocalisation in biological systems. *Sci Rep* 7: 8879, 2017.
30. Le Vasseur M, Chen VC, Huang K, Vogl WA and Naus CC: Pannexin 2 localizes at ER-mitochondria contact sites. *Cancers (Basel)* 11: 343, 2019.
31. Klionsky DJ, Abdel-Aziz AK, Abdelfatah S, Abdellatif M, Abdoli A, Abel S, Abeliovich H, Abildgaard MH, Abudu YP, Acevedo-Arozena A, *et al*: Guidelines for the use and interpretation of assays for monitoring autophagy (4th edition). *Autophagy* 17: 1-382, 2021.
32. Morciano G, Marchi S, Morganti C, Sbrano L, Bittremieux M, Kerkhofs M, Corricelli M, Danese A, Karkucinska-Wieckowska A, Wieckowski MR, *et al*: Role of mitochondria-associated ER membranes in calcium regulation in cancer-specific settings. *Neoplasia* 20: 510-523, 2018.
33. Murley A, Sarsam RD, Toulmay A, Yamada J, Prinz WA and Nunnari J: Ltc1 is an ER-localized sterol transporter and a component of ER-mitochondria and ER-vacuole contacts. *J Cell Biol* 209: 539-548, 2015.
34. Eisenberg-Bord M, Shai N, Schuldiner M and Bohnert M: A tether is a tether is a tether: Tethering at membrane contact sites. *Dev Cell* 39: 395-409, 2016.
35. Wang Z, Zhou H, Zheng H, Zhou X, Shen G, Teng X, Liu X, Zhang J, Wei X, Hu Z, *et al*: Autophagy-based unconventional secretion of HMGB1 by keratinocytes plays a pivotal role in psoriatic skin inflammation. *Autophagy* 17: 529-552, 2021.
36. Kim YH, Kwak MS, Lee B, Shin JM, Aum S, Park IH, Lee MG and Shin JS: Secretory autophagy machinery and vesicular trafficking are involved in HMGB1 secretion. *Autophagy* 17: 2345-2362, 2021.
37. Hu Y, Chen H, Zhang L, Lin X, Li X, Zhuang H, Fan H, Meng T, He Z, Huang H, *et al*: The AMPK-MFN2 axis regulates MAM dynamics and autophagy induced by energy stresses. *Autophagy* 17: 1142-1156, 2021.
38. Bjørkøy G, Lamark T, Brech A, Outzen H, Perander M, Overvatn A, Stenmark H and Johansen T: p62/SQSTM1 forms protein aggregates degraded by autophagy and has a protective effect on huntingtin-induced cell death. *J Cell Biol* 171: 603-614, 2005.
39. Komatsu M, Waguri S, Koike M, Sou YS, Ueno T, Hara T, Mizushima N, Iwata J, Ezaki J, Murata S, *et al*: Homeostatic levels of p62 control cytoplasmic inclusion body formation in autophagy-deficient mice. *Cell* 131: 1149-1163, 2007.
40. Pankiv S, Clausen TH, Lamark T, Brech A, Bruun JA, Outzen H, Øvervatn A, Bjørkøy G and Johansen T: p62/SQSTM1 binds directly to Atg8/LC3 to facilitate degradation of ubiquitinated protein aggregates by autophagy. *J Biol Chem* 282: 24131-24145, 2007.
41. Turkoz Uluer E, Kilicaslan Sonmez P, Akogullari D, Onal M, Tanriover G and Inan S: Do wortmannin and thalidomide induce apoptosis by autophagy inhibition in 4T1 breast cancer cells in vitro and in vivo? *Am J Transl Res* 13: 6236-6247, 2021.
42. Mauthe M, Orhon I, Rocchi C, Zhou X, Luhr M, Hijkema KJ, Coppes RP, Engedal N, Mari M and Reggiori F: Chloroquine inhibits autophagic flux by decreasing autophagosome-lysosome fusion. *Autophagy* 14: 1435-1455, 2018.
43. Wang D, Liu K, Fukuyasu Y, Teshigawara K, Fu L, Wake H, Ohtsuka A and Nishibori M: HMGB1 translocation in neurons after ischemic insult: Subcellular localization in mitochondria and peroxisomes. *Cells* 9: 643, 2020.
44. Jia L, Song Y, Song H, Wang G, Fan W, Li X, Zheng H and Yao A: Overexpression of high mobility group box 1 (HMGB1) has no correlation with the prognosis in glioma. *Biomark Med* 13: 851-863, 2019.
45. Fu L, Liu K, Wake H, Teshigawara K, Yoshino T, Takahashi H, Mori S and Nishibori M: Therapeutic effects of anti-HMGB1 monoclonal antibody on pilocarpine-induced status epilepticus in mice. *Sci Rep* 7: 1179, 2017.
46. Kostova N, Zlateva S, Ugrinova I and Pasheva E: The expression of HMGB1 protein and its receptor RAGE in human malignant tumors. *Mol Cell Biochem* 337: 251-258, 2010.
47. Taguchi A, Blood DC, del Toro G, Canet A, Lee DC, Qu W, Tanji N, Lu Y, Lalla E, Fu C, *et al*: Blockade of RAGE-amphoterin signalling suppresses tumour growth and metastases. *Nature* 405: 354-360, 2000.
48. Bald T, Quast T, Landsberg J, Rogava M, Glodde N, Lopez-Ramos D, Kohlmeyer J, Riesenberger S, van den Boorn-Konijnenberg D, Hömig-Hölzel C, *et al*: Ultraviolet-radiation-induced inflammation promotes angiogenesis and metastasis in melanoma. *Nature* 507: 109-113, 2014.
49. New J and Thomas SM: Autophagy-dependent secretion: Mechanism, factors secreted, and disease implications. *Autophagy* 15: 1682-1693, 2019.
50. Andersson U, Yang H and Harris H: High-mobility group box 1 protein (HMGB1) operates as an alarmin outside as well as inside cells. *Semin Immunol* 38: 40-48, 2018.
51. Elmaci I, Alturfan EE, Cengiz S, Ozpinar A and Altinoz MA: Neuroprotective and tumoricidal activities of cardiac glycosides. Could oleandrin be a new weapon against stroke and glioblastoma? *Int J Neurosci* 128: 865-877, 2018.
52. Fraser J, Simpson J, Fontana R, Kishi-Itakura C, Ktistakis NT and Gammoh N: Targeting of early endosomes by autophagy facilitates EGFR recycling and signalling. *EMBO Rep* 20: e47734, 2019.
53. Okuma Y, Becker LB, Hayashida K, Aoki T, Saeki K, Nishikimi M, Shoaib M, Miyara SJ, Yin T and Shinozaki K: Effects of post-resuscitation normoxic therapy on oxygen-sensitive oxidative stress in a rat model of cardiac arrest. *J Am Heart Assoc* 10: e018773, 2021.
54. Liu Y, Yan W, Tohme S, Chen M, Fu Y, Tian D, Lotze M, Tang D and Tsung A: Hypoxia induced HMGB1 and mitochondrial DNA interactions mediate tumor growth in hepatocellular carcinoma through Toll-like receptor 9. *J Hepatol* 63: 114-121, 2015.
55. Zhang GZ, Zhang K, Yang SQ, Zhang Z, Chen S, Hou BJ and Yuan JY: VASPIN reduces inflammation and endoplasmic reticulum stress of renal tubular epithelial cells by inhibiting HMGB1 and relieves renal ischemia-reperfusion injury. *Eur Rev Med Pharmacol Sci* 24: 8968-8977, 2020.
56. Tu L, Long X, Song W, Lv Z, Zeng H, Wang T, Liu X, Dong J and Xu P: MiR-34c acts as a tumor suppressor in non-small cell lung cancer by inducing endoplasmic reticulum stress through targeting HMGB1. *Oncotargets Ther* 12: 5729-5739, 2019.
57. Di Cara F, Andreoletti P, Tromprier D, Vejux A, Bülow MH, Sellin J, Lizard G, Cherkaoui-Malki M and Savary S: Peroxisomes in immune response and inflammation. *Int J Mol Sci* 20: 3877, 2019.
58. Lismont C, Revenco I and Fransen M: Peroxisomal hydrogen peroxide metabolism and signaling in health and disease. *Int J Mol Sci* 20: 3673, 2019.
59. Fan H, Tang HB, Chen Z, Wang HQ, Zhang L, Jiang Y, Li T, Yang CF, Wang XY, Li X, *et al*: Inhibiting HMGB1-RAGE axis prevents pro-inflammatory macrophages/microglia polarization and affords neuroprotection after spinal cord injury. *J Neuroinflammation* 17: 295, 2020.
60. Muro S: Alterations in cellular processes involving vesicular trafficking and implications in drug delivery. *Biomimetics (Basel)* 3: 19, 2018.
61. Nguyen TMT, Kim J, Doan TT, Lee MW and Lee M: APEX proximity labeling as a versatile tool for biological research. *Biochemistry* 59: 260-269, 2020.
62. Lam SS, Martell JD, Kamer KJ, Deerinck TJ, Ellisman MH, Mootha VK and Ting AY: Directed evolution of APEX2 for electron microscopy and proximity labeling. *Nat Methods* 12: 51-54, 2015.
63. Jiang J, Zhang L, Chen H, Lei Y, Zhang T, Wang Y, Jin P, Lan J, Zhou L, Huang Z, *et al*: Regorafenib induces lethal autophagy arrest by stabilizing PSAT1 in glioblastoma. *Autophagy* 16: 106-122, 2020.
64. Song L, Tang S, Han X, Jiang Z, Dong L, Liu C, Liang X, Dong J, Qiu C, Wang Y and Du Y: KIBRA controls exosome secretion via inhibiting the proteasomal degradation of Rab27a. *Nat Commun* 10: 1639, 2019.
65. Wall AA, Condon ND, Luo L and Stow JL: Rab8a localisation and activation by Toll-like receptors on macrophage macropinosomes. *Philos Trans R Soc Lond B Biol Sci* 374: 20180151, 2019.

66. Wu PH, Onodera Y, Giaccia AJ, Le QT, Shimizu S, Shirato H and Nam JM: Lysosomal trafficking mediated by Arl8b and BORC promotes invasion of cancer cells that survive radiation. *Commun Biol* 3: 620, 2020.
67. Tian X, Zheng P, Zhou C, Wang X, Ma H, Ma W, Zhou X, Teng J and Chen J: DIPK2A promotes STX17- and VAMP7-mediated autophagosome-lysosome fusion by binding to VAMP7B. *Autophagy* 16: 797-810, 2020.
68. Sleiman M, Stevens DR, Chitirala P and Rettig J: Cytotoxic granule trafficking and fusion in synaptotagmin7-deficient cytotoxic T lymphocytes. *Front Immunol* 11: 1080, 2020.



Copyright © 2023 Cui et al. This work is licensed under a Creative Commons Attribution-NonCommercial-NoDerivatives 4.0 International (CC BY-NC-ND 4.0) License.